Molecular Crystals and Liquid Crystals

Publication details, including instructions for authors and subscription information:
http://www.tandfonline.com/loi/gmcl20

Hydrodynamic of Active Liquid Crystals: A Hybrid Lattice Boltzmann Approach

E. Orlandini [a] , M. E. Cates [b] , D. Marenduzzo [b] , L. Tubiana [a b] & J. M. Yeomans [c]

[a] Dipartimento di Fisica and Sezione INFN, Universita' di Padova, Padova, Italy

[b] SUPA, School of Physics, University of Edinburgh, Edinburgh, Scotland

[c] The Rudolf Peierls Centre for Theoretical Physics, Oxford, England

Version of record first published: 05 Apr 2011

To cite this article: E. Orlandini, M. E. Cates, D. Marenduzzo, L. Tubiana & J. M. Yeomans (2008): Hydrodynamic of Active Liquid Crystals: A Hybrid Lattice Boltzmann Approach, Molecular Crystals and Liquid Crystals, 494:1, 293-308

To link to this article: http://dx.doi.org/10.1080/15421400802430117

Mol. Cryst. Liq. Cryst., Vol. 494, pp. 293–308, 2008

ISSN: 1542-1406 print/1563-5287 online
DOI: 10.1080/15421400802430117

Taylor & Francis
Taylor & Francis Group

Hydrodynamic of Active Liquid Crystals: A Hybrid Lattice Boltzmann Approach

E. Orlandini[1], M. E. Cates[2], D. Marenduzzo[2], L. Tubiana[1,2], and J. M. Yeomans[3]
[1]Dipartimento di Fisica and Sezione INFN, Universita' di Padova, Padova, Italy
[2]SUPA, School of Physics, University of Edinburgh, Edinburgh, Scotland
[3]The Rudolf Peierls Centre for Theoretical Physics, Oxford, England

Active gels or active liquid crystals are soft materials which are driven out of equilibrium by their continuum use of chemical energy. Physical realisations of active gels are solutions of cytoskeletal filaments with molecular motors, and concentrated suspensions of bacterial swimmers. Here we focus on the active nematic phase which is exhibited by these materials, and study their hydrodynamics when confined in a slab of a finite height. We solve the hydrodynamic equations of motion by means of a hybrid lattice Boltzmann algorithm. The homogeneous flow is known to be unstable for sufficiently large activity, leading to a state with spontaneous flow in steady state. We characterise the form of this flow in 1 and 2 dimensions with extensile and contractile flow aligning materials.

INTRODUCTION

Active viscoelastic gels and active liquid crystals are a challenging class of soft materials that have recently attracted a lot of theoretical and experimental attention [1–5]. They differ from their passive counterparts in the crucial respect that they continuously burn energy, e.g., from chemical reactions, which drives them out of thermodynamic equilibrium even in steady state. Examples of passive viscoelastic fluids are polymeric fluids, rubber, molten plastics etc. Examples of active gels are cytoskeletal slabs [6,7], biomimetic systems [8] or solutions of molecular motors such as dyneins or myosins and microtubules or actin

Thanks for the financial support of the European Community-Research Infrastructure Action under the FP6 "Structuring the European Research Area" program.

Address correspondence to E. Orlandini, Departimento di Fisica and Sezione INFN, Universita' di Padova, Via Marzolo 8, Padova 35131, Italy. E-mail: orlandini@pd.infn.it

fibers [6–11]. In these solutions the molecular motors interact with actin or microtubules by exerting forces and or torques on them, creating motile and transient cross-links etc. It is the presence of the molecular motors, which are able to use chemical energy to perform mechanical work, which renders these viscoelastic polymeric fluids 'active'. The source of chemical energy in such active gels typically comes from ATP hydrolysis (there is estimated to be $\sim 15\,k_BT$ worth of biochemical energy from each ATP hydrolysis reaction).

Activity imparts non-trivial physical properties. Perhaps the most striking is that spontaneous flow can exist in non-driven active materials [1–5], in sharp contrast to their passive liquid crystalline counterparts. Thus such materials, while always remaining active in a microscopic sense, can undergo a phase transition from a passive phase (where activity is macroscopically incoherent) to an active phase (exhibiting spontaneous flow). Furthermore, many biological gels, such as actin and neurofilament networks, thicken when sheared [12]. This is the opposite of the typical behaviour of viscous polymeric fluids such as molten plastics, which flow more easily as pressure increases. Activity has been suggested to be amongst the possible causes of this peculiar flow response [4,13].

In this paper we present a series of hybrid lattice Boltzmann simulations of the hydrodynamic equations of motion of an active nematic liquid crystal. Numerical methods are needed in this, as the insight which is possible to obtain analytically is limited although important. For instance, it has been possible to theoretically predict [2] by analytic methods the existence of an activity-induced transition between a passive phase with no local flow to an 'active' phase, in which the fluid is flowing at steady state. However, as the techniques used thus far essentially allow a stability analysis of the problem in selected geometries, it is not possible to predict e.g., the flowing and director field patterns deep in the active phase, away from the transition to spontaneous flow. Furthermore, using a numerical method allows us to consider more detailed forms for the equations of motion. Thus here we extend the vector polarisation model considered analytically in Refs. [1,2], to a tensorial equivalent (similar to the one introduced in Refs. [3,4]), which allows us to study situations in which the order parameter is not constant throughout the sample so that defects are automatically incorporated, as is flow-induced or paranematic ordering. We can also describe biaxial ordering.

We consider the specific case of a material that is sandwiched between two infinite parallel planes placed at mutual distance L and at which the director field is anchored along one of the directions in the plane (homogeneous anchoring). If translation invariance along

the plane directions is assumed a quasi-1D geometry is studied. With this geometry we observe a phase transition between a passive and an active phase when the "activity" ζ, a parameter which measures the coupling between pressure tensor and order parameter, exceeds in absolute value a finite threshold. We estimate the active phase diagram for different values of L and show that the critical activity scale as L^{-2} for this geometry.

Finally, we consider a quasi-2D case of an extensile flow-aligning active liquid crystal film, wrapped on a cylindrical surface (i.e., with periodic boundary conditions). Our simulations show that there are additional instabilities in this geometry. Spontaneous flow this time appears as convection rolls, which, deeper in the active phase, transiently increase in number and eventually split up leading to a highly distorted flowing director field pattern.

Interestingly, while for quasi-1D systems and flow aligning materials the transition to a steady state with a spontaneous flow exists only for extensile rods, in the quasi-2D case it occurs also for sufficiently contractile ones. (Here "extensile" means tending to propel fluid outwards along the long axis or molecular director n, drawing it in radially on the midplane, while "contractile" means the opposite [4].)

MODELS AND INTEGRATION METHODS

Equations of Motion

We consider the formulation of liquid crystal hydrodynamics given by Beris and Edwards [14–16], generalized for active liquid crystals.

The equations of motion are written in terms of a tensor order parameter $\mathbf{Q}$ which is related to the direction of individual molecules, $\hat{\boldsymbol{n}}$, by $Q_{\alpha\beta} = \langle \hat{n}_\alpha \hat{n}_\beta - 1/3\delta_{\alpha\beta} \rangle$ where the angular brackets denote a coarse-grained average and the Greek indices label the Cartesian components of $\mathbf{Q}$. The tensor $\mathbf{Q}$ is traceless and symmetric. Its largest eigenvalue, $2/3q,\ 0 < q < 1$, describes the magnitude of the order.

The equilibrium properties of the liquid crystal in its passive state are described by a Landau-de Gennes free energy density. This comprises a bulk term (summation over repeated indices is implied hereafter),

$$\mathcal{F}_b = \frac{A_0}{2}\left(1 - \frac{\gamma}{3}\right)Q_{\alpha\beta}^2 - \frac{A_0\gamma}{3}Q_{\alpha\beta}Q_{\beta\gamma}Q_{\gamma\alpha} + \frac{A_0\gamma}{4}(Q_{\alpha\beta}^2)^2, \tag{1}$$

which describes a first-order transition from the isotropic to the nematic phase at $\gamma = 2.7$, together with a distortion term, which we take in a (standard) one-constant approximation as [17]

$$\mathcal{F}_d = \frac{K}{2}(\partial_\beta Q_{\alpha\beta})^2, \tag{2}$$

In the equations above, A_0 is a constant, γ controls the magnitude of order (it may be viewed as an effective temperature or concentration for thermotropic and lyotropic liquid crystals respectively), while K is an elastic constant.

The anchoring of the director field on the boundary surfaces (see Fig. 2) is ensured by adding a pinning term

$$f_S = \frac{1}{2}W_0(Q_{\alpha\beta} - Q^0_{\alpha\beta})^2 \tag{3}$$

with $Q^0_{\alpha\beta}$ typically of the form

$$Q^0_{\alpha\beta} = S_0(n^0_\alpha n^0_\beta - \delta_{\alpha\beta}/3). \tag{4}$$

The parameter W_0 controls the strength of the anchoring, while S_0 determines the magnitude of surface order. If the surface order is equal to the bulk order (as is the case in the simulations reported here), S_0 should be taken equal to q, the order parameter in the bulk. In what follows we will consider strong anchoring (W_0 large).

The equation of motion for $\mathbf{Q}$ is [14]

$$(\partial_t + \vec{u}\cdot\nabla)\mathbf{Q} - \mathbf{S}(\mathbf{W},\mathbf{Q}) = \Gamma\mathbf{H} + \lambda\mathbf{Q} \tag{5}$$

where Γ is a collective rotational diffusion constant, and λ is an 'activity' parameter of the liquid crystal.

The first term on the left-hand side of Eq. (5) is the material derivative describing a quantity advected by a fluid with velocity $\vec{u}$. This is generalized for rod-like molecules by a second term

$$\begin{aligned}\mathbf{S}(\mathbf{W},\mathbf{Q}) =&(\xi\mathbf{D}+\omega)(\mathbf{Q}+\mathbf{I}/3) + (\mathbf{Q}+\mathbf{I}/3)(\xi\mathbf{D}-\omega)\\ &- 2\xi(\mathbf{Q}+\mathbf{I}/3)\mathrm{Tr}(\mathbf{Q}\mathbf{W})\end{aligned} \tag{6}$$

where Tr denotes the tensorial trace, while $\mathbf{D} = (\mathbf{W}+\mathbf{W}^T)/2$ and $\omega = (\mathbf{W}-\mathbf{W}^T)/2$ are the symmetric part and the anti-symmetric part respectively of the velocity gradient tensor $W_{\alpha\beta} = \partial_\beta u_\alpha$. The constant ξ depends on the molecular details of a given liquid crystal. In our context increasing ξ tends to disfavour tumbling and favour aligning of the director in the material. The molecular field $\mathbf{H}$ in Eq. (5) is given by $\mathbf{H} = -\frac{\delta\mathcal{F}}{\delta\mathbf{Q}} + (\mathbf{I}/3)\mathrm{Tr}\frac{\delta\mathcal{F}}{\delta\mathbf{Q}}$ where $\mathcal{F} = \mathcal{F}_b + \mathcal{F}_d$. The term proportional to λ is specific of an active material and describes the self-alignment contribution due to the adsorbed (internal or external) energy.

The fluid velocity, $\vec{u}$, obeys the continuity equation and the Navier-Stokes equation,

$$\rho(\partial_t + u_\beta \partial_\beta) u_\alpha = \partial_\beta(\Pi_{\alpha\beta}) + \eta \partial_\beta(\partial_\alpha u_\beta + \partial_\beta u_\alpha), \tag{7}$$

where ρ is the fluid density, η an isotropic viscosity and $\Pi_{\alpha\beta} = \Pi^{\text{passive}}_{\alpha\beta} + \Pi^{\text{active}}_{\alpha\beta}\Pi^{\text{passive}}_{\alpha\beta}$ is the stress tensor necessary to describe ordinary liquid crystal hydrodynamics:

$$\begin{aligned}\Pi^{\text{passive}}_{\alpha\beta} = &- P_0\delta_{\alpha\beta} + 2\xi\left(Q_{\alpha\beta} + \frac{1}{3}\delta_{\alpha\beta}\right)Q_{\gamma\epsilon}H_{\gamma\epsilon} \\ &- \xi H_{\alpha\gamma}\left(Q_{\gamma\beta} + \frac{1}{3}\delta_{\gamma\beta}\right) - \xi\left(Q_{\alpha\gamma} + \frac{1}{3}\delta_{\alpha\gamma}\right)H_{\gamma\beta} \\ &- \partial_\alpha Q_{\gamma\nu}\frac{\delta\mathcal{F}}{\delta\partial_\beta Q_{\gamma\nu}} + Q_{\alpha\gamma}H_{\gamma\beta} - H_{\alpha\gamma}Q_{\gamma\beta}.\end{aligned} \tag{8}$$

The P_0 term is, to a good approximation, constant in the simulations reported here. The active term is given by

$$\Pi^{\text{active}}_{\alpha\beta} = -\zeta Q_{\alpha\beta}, \tag{9}$$

where ζ is another 'activity' parameter [1,2,4]. Note that with the sign convention chosen here $\zeta > 0$ corresponds to extensile rods and $\zeta < 0$ to contractile ones [4]. As in Eq. (5), the contribution of activity to the stress tensor entering Eq. (7) is considered at the lowest in $\mathbf{Q}$ and has been previously proposed on the basis of symmetry, and of the analysis of a fluid of contractile or extensile dipolar objects in [4]. A similar term can also be derived by coarse graining a more microscopic model for a solution of actin fibers and myosins as in Ref. [5].

Clearly, the model above reduces for $\lambda = \zeta = 0$ to the Beris-Edwards model for liquid crystal hydrodynamics. For uniaxial active liquid crystals, the director field $\vec{n}$ is well defined through $Q_{\alpha\beta} = 3q(n_\alpha n_\beta - \delta_{\alpha\beta}/3)/2$. In this limit our model can be shown to reduce to the vectorial model considered in [1,2,18]. In particular the analytical prediction of the phase boundary in the (ζ, λ) plane, for an active nematic confined between parallel planes at separation L, found in Ref. [2], becomes for our model

$$\zeta L^2 = \frac{12\pi^2 K(12\tau_f\,\Gamma - 5\cdot\xi q^2 - 14\cdot\xi q + \xi + \xi^2 q^2 + 4\cdot\xi^2 + 4\cdot\xi^2 q + 9\cdot q^2)}{9(\xi q + 2\cdot\xi - 3\cdot q)}. \tag{10}$$

From Eq. (10) it is apparent that the critical activity threshold beyond which spontaneous flow is found scales like L^{-2}, and thus vanishes for an infinite system. Note that the dependence on λ of the phase boundary is indirect, via q.

To fully understand the physical origin of the phenomenological couplings ζ and λ, as well as of the range of values these may attain in physically relevant situations, a multi-scale modelling at different coarse graining levels and more accurate quantitative experiments are required. However, experiments already show that actomyosin gels are contractile, so that in physiological conditions those materials should be described by negative values of ζ [19]. The term proportional to λ has been proposed in Ref. [4] as a symmetry allowed term which, for dilute bacterial suspensions, should be negative and proportional to the inverse of the time scale for relaxation of activity-induced ordering. In Ref. [2] it was pointed out that, instead, $\lambda > 0$ when describing concentrated actomyosin gels and other systems which display zipping or other self-alignment effects (this is relevant for the cases considered in [20]).

The Hybrid Lattice Boltzmann Algorithm

The equations of motion (5) and (7) can be integrated numerically by implementing a generalization [13] of the Lattice Boltzmann (LB) algorithm [21] introduced in Ref. [22] and successfully used to study a number of problems in the hydrodynamics and rheology of a passive liquid crystal.

Here we use a different approach in which Eq. (5) is solved via a finite difference predictor-corrector algorithm, while the lattice Boltzmann algorithm is devoted to the integration of the Navier-Stokes equation, (7). With respect to a full LB approach [22,23], the primary advantage of this hybrid method is that it will allow simulations of larger systems as it involves consistently smaller memory requirements. Indeed, while in a full LB treatment one has to store 6 sets of 15 distribution functions at any lattice point (if we choose the 3DQ15 velocity vector lattice [21] as we do here (see Fig. 1)), in the hybrid approach just one set of distribution functions plus the five independent components of the $\mathbf{Q}$ tensor are needed. The hybrid method is also numerically more stable since it avoids the error term arising in the Chapman-Enskog expansion used to connect the LB model to the order parameter evolution equation in the continuum limit [23].

Let us describe first how to integrate the Navier-Stokes equations by the Lattice Boltzmann algorithm. This is defined in terms of a single set of partial distribution functions, the scalars $f_i(\vec{x})$, that sum on each lattice site $\vec{x}$ to give the density. Each f_i is associated with a lattice vector $\vec{e}_i$ [22]. We choose a 15-velocity model on the cubic lattice with lattice vectors (see Fig. 1):

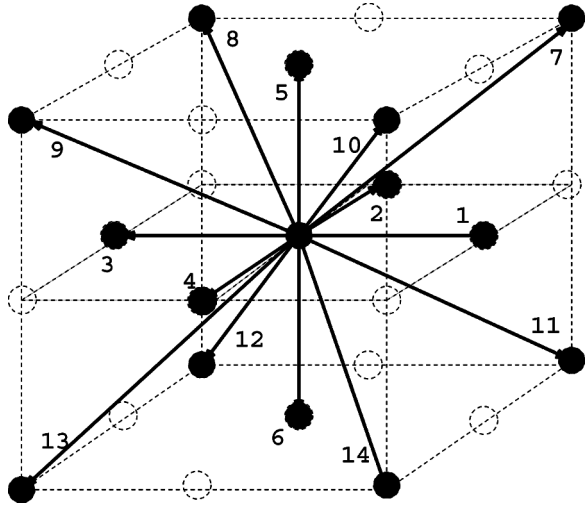

FIGURE 1 The 3DQ15 velocity vector lattice used in our lattice Boltzmann algorithm.

$$\vec{e}_i^{(0)} = (0,0,0) \tag{11}$$

$$\vec{e}_i^{(1)} = (\pm 1,0,0),(0,\pm 1,0),(0,0,\pm 1) \tag{12}$$

$$\vec{e}_i^{(2)} = (\pm 1,\pm 1,\pm 1). \tag{13}$$

The indices, i, are ordered so that $i=0$ corresponds to $\vec{e}_i^{(0)}$, $i=1,\ldots,6$ correspond to the $\vec{e}_i^{(1)}$ set and $i=7,\ldots,14$ to the $\vec{e}_i^{(2)}$ set.

Physical variables are defined as moments of the distribution functions:

$$\rho = \sum_i f_i, \qquad \rho u_\alpha = \sum_i f_i e_{i\alpha}. \tag{14}$$

The distribution functions evolve in a time step Δt according to

$$f_i(\vec{x}+\vec{e}_i\Delta t, t+\Delta t) - f_i(\vec{x},t) = \frac{\Delta t}{2}\left[C_{fi}(\vec{x},t,\{f_i\}) + C_{fi}(\vec{x}+\vec{e}_i\Delta t, t+\Delta t, \{f_i^*\})\right]. \tag{15}$$

This represents free streaming with velocity $\vec{e}_i$ followed by a collision step which allows the distributions to relax towards equilibrium.

The f_i^*'s are first order approximations to $f_i(\vec{x}+\vec{e}_i\Delta t, t+\Delta t)$, and they are obtained by using $\Delta t\ \mathcal{C}_{fi}(\vec{x},\ t,\ \{f_i\})$ on the right hand side of Eq. (15). Discretizing in this way, which is similar to a predictor-corrector scheme, has the advantages that lattice viscosity terms are eliminated to second order and that the stability of the scheme is improved [23].

The collision operators are taken to have the form of a single relaxation time Boltzmann equation, together with a forcing term

$$\mathcal{C}_{fi}(\vec{x},\ t, \{f_i\}) = -\frac{1}{\tau_f}(f_i(\vec{x},\ t) - f_i^{eq}(\vec{x},\ t, \{f_i\})) + p_i(\vec{x},\ t, \{f_i\}), \tag{16}$$

The form of the equations of motion follow from the choice of the moments of the equilibrium distributions f_i^{eq} and the driving terms p_i. Moreover, f_i^{eq} is constrained by

$$\sum_i f_i^{eq} = \rho, \qquad \sum_i f_i^{eq} e_{i\alpha} = \rho u_\alpha, \qquad \sum_i f_i^{eq} e_{i\alpha} e_{i\beta} = -\sigma_{\alpha\beta} + \rho u_\alpha u_\beta \tag{17}$$

where the zeroth and first moments are chosen to impose conservation of mass and momentum. The second moment of f^{eq} is determined by $\sigma_{\alpha\beta}$, which is the symmetric part of the stress tensor $\Pi_{\alpha\beta}$, not including the double gradient term, $\partial_\alpha \boldsymbol{Q}_{\gamma\nu} \frac{\delta\mathcal{F}}{\delta\partial_\beta \boldsymbol{Q}_{\gamma\nu}}$. The divergences of $\tau_{\alpha\beta}$ and of $\partial_\alpha \boldsymbol{Q}_{\gamma\nu} \frac{\delta\mathcal{F}}{\delta\partial_\beta \boldsymbol{Q}_{\gamma\nu}}$ instead enter effectively as a body force:

$$\sum_i p_i = 0, \quad \sum_i p_i e_{i\alpha} = \partial_\beta \tau_{\alpha\beta} - \partial_\beta\left(\partial_\alpha \boldsymbol{Q}_{\gamma\nu} \frac{\delta\mathcal{F}}{\delta\partial_\beta \boldsymbol{Q}_{\gamma\nu}}\right), \quad \sum_i p_i e_{i\alpha} e_{i\beta} = 0, \tag{18}$$

where $\tau_{\alpha\beta}$ denotes the anti-symmetric part of the stress tensor.

Conditions (17)–(18) are satisfied by writing the equilibrium distribution functions and forcing terms as polynomial expansions in the velocity.

$$\begin{aligned} f_i^{eq} = {} & A_s + B_s u_\alpha e_{i\alpha} + C_s u^2 + D_s u_\alpha u_\beta e_{i\alpha} e_{i\beta} + E_{s\alpha\beta} e_{i\alpha} e_{i\beta} \\ & + P_s \partial_\beta \left[\tau_{\alpha\beta} - \left(\partial_\alpha \boldsymbol{Q}_{\gamma\nu} \frac{\delta\mathcal{F}}{\delta\partial_\beta \boldsymbol{Q}_{\gamma\nu}}\right)\right] e_{i\alpha}, \end{aligned} \tag{19}$$

where $s = \vec{e}_i^{\,2} \in \{0, 1, 2\}$ identifies separate coefficients for different absolute values of the velocities (i.e., s denotes the absolute value of the square of the velocity vectors).

The coefficients in the expansion are (in general non-uniquely) determined by the requirements that these constraints are fulfilled. A possible choice is given below:

$$A_2 = \frac{\rho T}{10}, \quad A_1 = A_2, \quad A_0 = \rho - 14A_2,$$
$$B_2 = \rho/24, \quad B_1 = 8B_2,$$
$$C_2 = -\frac{\rho}{24}, \quad C_1 = 2C_2, \quad C_0 = -\frac{2\rho}{3},$$
$$D_2 = \frac{\rho}{16}, \quad D_1 = 8D_2$$
$$E_{2\alpha\beta} = -\frac{1}{16}\left(\Pi_{\alpha\beta} - \frac{\sigma_{\gamma\gamma}}{3}\delta_{\alpha\beta}\right), \quad E_{1\alpha\beta} = 8E_{2\alpha\beta}$$
$$P_2 = \frac{1}{24}, \quad P_1 = 8P_2. \tag{20}$$

The active contributions simply alter the constraints on the second moment of the f_i's since $\Pi_{\alpha\beta} = \Pi^{\text{passive}}_{\alpha\beta} + \Pi^{\text{active}}_{\alpha\beta}$.

Clearly the stress tensor $\Pi_{\alpha\beta}$ is a function of $Q_{\alpha\beta}$ and, in the hybrid approach, the coefficients $E_{2\alpha\beta}$ and $E_{1\alpha\beta}$ of the f_i^{eq}'s are computed by using the solution (via finite difference methods) of the coupled Eq. (5). This differs from the fully LB treatment of nematics; see Refs. [22,23].

RESULTS

All the results we present in this work refer to an active LC in the nematic phase that is confined between two plates at separation L along the z direction (Fig. 2). From now on we will refer to the angle between the director field and the positive y direction as the polarization angle, θ, the convention being that $\theta > 0$ if the positive y axis can be superimposed with the director field with an anti-clockwise rotation

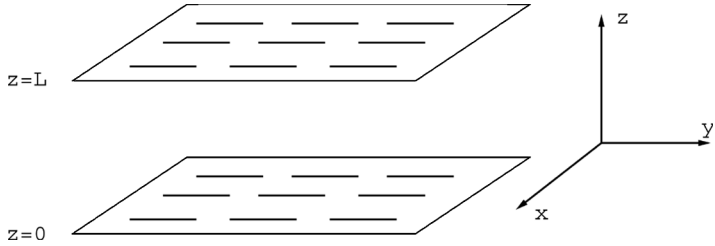

FIGURE 2 Geometry used for the calculations described in the text. The active gel is sandwiched between two infinite plates, parallel to the xy plane, lying at $z = 0$ and $z = L$. We consider homogeneous parallel anchoring. This geometry is known as the Freedericksz cell in passive liquid crystal device.

of an angle $|\theta|$ (which is defined to be smaller than π), around the x axis. For simplicity we restrict ourselves to homogeneous anchoring where the polarization at the boundaries is parallel to the y-direction, $\theta = 0$ (Fig. 2) (This geometry is known as the Freedericksz cell in passive liquid crystal device terminology, [17]). In what follows we will mainly report parameter values in simulation units. These can be straightforwardly related to physical units by noting that one space and time simulation unit correspond to $0.05\,\mu$m and $0.67\,\mu$s respectively, if we choose the values of the rotational viscosity γ_1 [17] and of the elastic constant K to be 1 Poise and 5 pN respectively. For definiteness we now fix $\tau_f = 2.5$, $A_0 = 0.1$, $K = 0.04$, $\Gamma \sim 0.34$, $\gamma = 3$ and $\xi = 0.7$. Fixing ξ to a value bigger than 0.6 corresponds to consider flow aligning material. Unless otherwise stated, the only parameters that will vary in the simulations are then L, λ and ζ.

Comparison of Hybrid with Conventional LB Codes

In Figure 3 we show the time evolution of the director and velocity at $z = L/4$ (in the geometry of Fig. 2) and in the mid-plane respectively, computed via the hybrid algorithm and via a full LB algorithm (as described in Refs. [22,23] for passive nematics and in [13] for the active case). The agreement proves the validity of our hybrid approach. Note that two full LB algorithms are benchmarked against the hybrid code. In one case the double gradient term is entered as a constraint in the

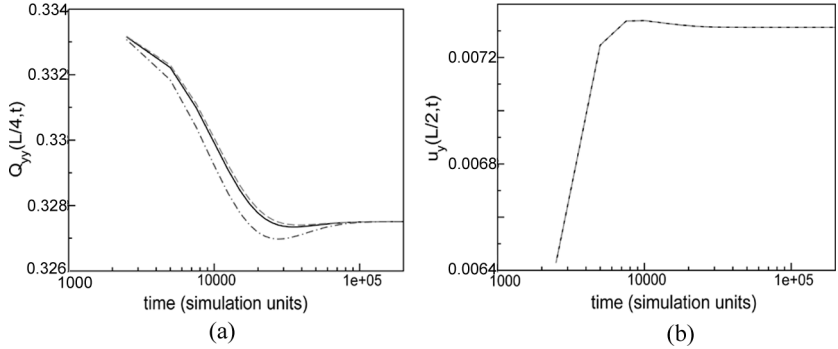

FIGURE 3 Time evolution of Q_{yy} at $z = L/4$ (a) and of u_y in the mid-plane (b), as predicted by our hybrid LB treatment (solid black lines), and by two types of full LB treatment (dashed red lines, with the double gradient terms entered in the first moment constraint, to avoid spurious velocities at equilibrium; and dot-dashed blue lines, with the double gradient term entered in the second moment constraint).

second moment, in the other its derivative is entered as a body force (see Eq. (19)). Note that the latter procedure guarantees that no spurious velocities are found in steady state, see e.g., Ref. [24]. It can be seen that the LB treatment with the double gradient terms entered in the second moment constraint leads to a small deviation at intermediate times. This is a discretisation error that is known to occur, for this method, in 2D giving rise to small spurious velocities even in the steady state [24].

Spontaneous Flow in a Quasi 1D System

We first consider a quasi-1D system in which translational invariance along x and y is assumed for the geometry of Figure 2.

Figure 4 shows the behaviour in the (λ, ζ) plane for three different system sizes $L = 50$, $L = 100$ and $L = 200$. We confirm the presence of a transition between a passive and an active phase, predicted analytically in Refs. [1,2]. In the passive phase, which occurs for small system sizes or for small values of the activity ζ, there is no flow and the polarisation field is homogeneous. The active phase is characterized instead

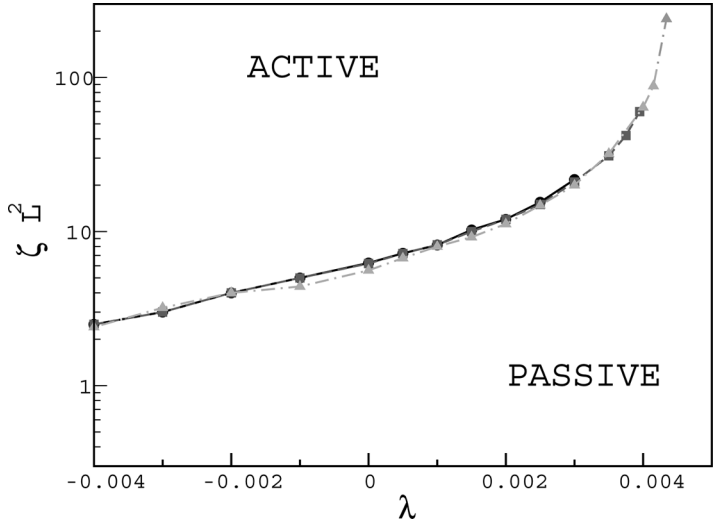

FIGURE 4 Boundary corresponding to the onset of spontaneous flow in the (λ, ζ) plane for an active liquid crystal, for three different system sizes ($L = 50,100,200$). Parameters are $\xi = 0.7$, $\gamma = 3$ corresponding to a flow aligning nematic. Notice that by rescaling ζ to ζL^2 all the data collapse into a single curve.

by the presence of a spontaneous flow along x which is initially approximately sinusoidal with a half wavelength between the channel walls. If one multiplies the critical values ζ_c by L^2 the data collapse into a single curve, confirming the scaling relation of Eq. (10). This also suggests that the system can reach an active state either by increasing the activity parameter or by increasing the distance between the confining plates making the boundary effects less effective. The steady states solutions in the active phase can be explored by looking at the flow field and director orientation profiles displayed by the system at sufficiently late times (see Fig. 5).

By means of a stability analysis, valid very close to the phase boundary, an analytic expression for $u_y(z)$ was found in [2]. This predicts a sinusoidal modulation with a node at the centre of the channel. While our numerics shows this solution to be metastable for a long time close to the threshold, the eventual steady state we find is a quasi-Poiseuille flow with a maximum at the centre of the channel (Fig. 5a) whose value increases as we go deep into the active phase (i.e., as ζ increases). Hence, with homogeneous boundary conditions and translational invariance along the flow direction the active gel displays a spontaneous net mass flux, in contrast with the balancing fluxes of forward and backward fluid in the two halves of the cell, predicted in [2]. The direction of the mass flux is chosen by spontaneous symmetry breaking or, in practice, small deviations from symmetry between y and $-y$ in the initial condition. Note that for a fixed initial condition as selected above, the flow direction can also switch on

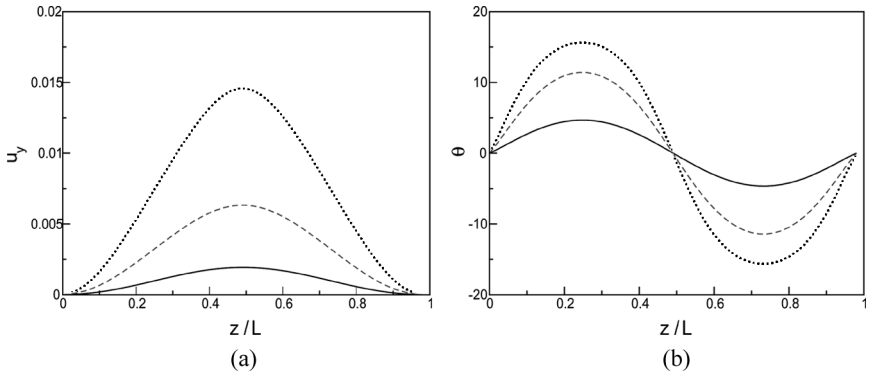

FIGURE 5 Velocity (left) and polarization (right) fields in steady state for an active liquid crystal slab with homogeneous anchoring at the boundaries, $\lambda = -0.002$ and ζ equal to 0.003 (solid line), 0.005 (long-dashed line), and 0.006 (dotted line), respectively. Other parameters are as specified in the text.

variation in ζ: to ease comparisons, some such switches are silently reversed in Figure 5. It is important to stress that the phase diagram in Figure 4 and the spontaneous flow profiles of Figure 5 have been obtained for *flow aligning* ($\xi > 0.6$) *extensile* ($\zeta > 0$) systems. For *flow aligning* ($\xi > 0.6$) *contractile* ($\zeta < 0$) systems the quasi-1D geometry does not allow the onset of a spontaneous flow. In order to observe a spontaneous flow for contractile rods in a quasi-1D geometry *flow tumbling* materials have to be considered [18].

Spontaneous Flow in Two Dimensions

Thus far, all simulations reported here were performed in a quasi-1D geometry, where translational invariance is assumed along x and y. The same simplification is often employed in numerical studies of passive liquid crystals (see many examples in Ref. [17]); moreoever, as shown above they allowed us to check detailed analytical predictions (calculated at director-field or Ericksen-Leslie level) made in exactly this geometry [2]. It is clearly important and interesting to consider whether there are additional spontaneous flow instabilities in a higher dimensionality. With periodic boundary conditions such instabilities must spontaneously break the translational invariance in x and y. The setup is still the one sketched in Figure 2 with $L_z = 100$, $L_y = 100$ and $L_x = 0$. Translational invariance along x is maintained but periodic boundary conditions are used to allow breakdown of this along the flow direction, y. We considered initial conditions with the director field along the y direction except for points along the midplane $z = L/2$, in which there was an alternating tilt of $\pm 10^\circ$ in stripes (the width of the initial stripes did not affect the steady state reached at the end of the simulations).

Active Extensile

Some results for the active extensile case in 2 dimensions were reported in Ref. [18] (see e.g., Fig. 16 of Ref. [18] – another example, with different ζ and A_0, is shown in Fig. 6). For low values of the activity, spontaneous flow appears as a pair of convection rolls which lead to a splay-bend in-plane deformation of the director field profile. The order parameter is to a good approximation constant ($q \simeq 0.5$) throughout the sample. The threshold at which the spontaneous flow occurs is smaller than the one found in the quasi-1D simulation. This is due to the fact that along y effectively homeotropic anchoring conditions are seen, and the active phase is entered for a smaller value of ζ in this geometry. Note that, since at onset of the convection rolls there are exactly two of these in the periodic cell, the details of the

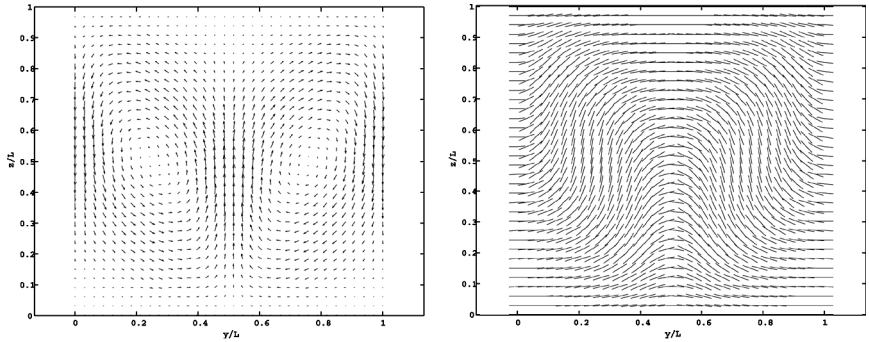

(a) (b)

FIGURE 6 Maps of velocity field (a) and director field (b) in steady state for an active extensile aligning liquid crystal ($\zeta = 0.002$ and $A_0 = 1$), simulated on a two-dimensional $L = 100 \times L = 100$ grid.

transition and the steady states in the active phase may now depend sensitively on the aspect ratio of the cell.

As the system goes deeper into the active phase, the number of convection rolls is, at early times in the simulations, larger [18]. These convection rolls then split up, and the flow field acquires an out-of-plane component (i.e., there is flow along the x direction). After this happens, a number of vortices form which lead to a complicated flow accompanied by the formation of defects (of topological strength $\pm 1/2$) in the director field profile.

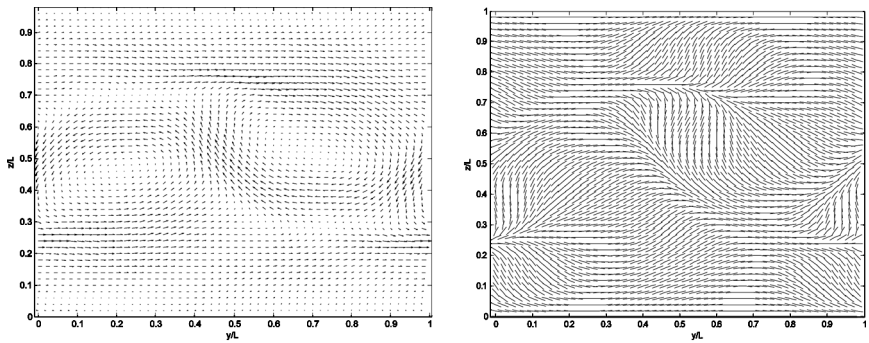

(a) (b)

FIGURE 7 Maps of velocity field (a) and director field (b) in steady state for an active contractile aligning liquid crystal ($\zeta = -0.001$), simulated on a two-dimensional $L = 100 \times L = 100$ grid.

Active Contractile

Figure 7 shows the late time flow and director fields for a contractile ($\zeta = -0.001$) flow aligning system. Unlike the quasi-1D system with homogeneous anchoring the 2D contractile flow aligning material displays a spontaneous flow. As for the extensile case this flow is organized in terms of convective, although much more distorted, rolls. Also the director field at steady state is more structured than in the extensile system but the splay bend in-plane deformations are still present.

CONCLUSIONS AND DISCUSSIONS

In conclusions, we have presented an hybrid lattice Boltzmann algorithm to investigate numerically the hydrodynamic properties of an active (flow-aligning) liquid crystalline fluid. In the equations we use the orientational degrees of freedom are characterised by a tensorial order parameter. This renders the algorithm general enough to deal – in principle – with non-homogeneous, flow-induced or paranematic ordering, as well as with topological defects.

We have first considered a quasi-1D geometry where the system is confined into a slab of width L and the director field is constrained to lie along a common direction along both confining plates. With this setting we show that our algorithm gives a non-equilibrium transition from a passive to an active phase, and that this occurs with an activity threshold that scales as L^{-2}. We have then considered how the director and flow fields in steady state evolve upon increasing the parameter ζ, which is a measure of the liquid crystal 'activity'.

Finally, we performed two-dimensional simulations, with periodic boundary conditions along the y direction and planar anchoring along that direction on both confining plates. Because of the additional instabilities that are present in a quasi-2D geometry the transition to a spontaneous flow is richer than the one we found for the quasi-1D case and it occurs for contractile flow aligning materials as well. Moreover, deep into the active phase, where non linear effects become important, a spontaneous flow also along the x direction (out of the plane spontaneous flow) is observed in this geometry.

Our algorithm is quite flexible and can be generalized in several ways. For instance, an additional order parameter equation, describing the time evolution of a polar vector field, can be considered with little more effort. This would allow a full 2D study of polar active nematics [5] with a variable degree of ordering. The algorithm can be either straightforwardly applied to 3D problems or used to explore

the rheological properties of active gels either deep in the nematic phase or close to the isotropic-nematic transition point.

REFERENCES

[1] Kruse, K., Joanny, J. F., Julicher, F., Prost, J., & Sekimoto, K. (2005). *Eur. Phys. J. E*, *16*, 5; (2004). *Phys. Rev. Lett.*, *92*, 078101.
[2] Voituriez, R., Joanny, J. F., & Prost, J. (2005). *Europhys. Lett.*, *70*, 404; (2006). *Phys. Rev. Lett.*, *96*, 028102.
[3] Simha, R. A. & Ramaswamy, S. (2002). *Phys. Rev. Lett.*, *89*, 058101.
[4] Hatwalne, Y., Ramaswamy, S., Rao, M., & Simha, R. A. (2004). *Phys. Rev. Lett.*, *92*, 118101.
[5] Liverpool, T. B. & Marchetti, M. C. (2001). *Phys. Rev. Lett.*, *90*, 138102; (2005). *Europhys. Lett.*, *69*, 846.
[6] Bray, D. (2000). *Cell Movements: From Molecules to Motility*, Garland Publishing: New York.
[7] Howard, J. (2001). *Mechanics of Motor Proteins and the Cytoskeleton*, Sinauer Associates, Inc.: Sunderland.
[8] van der Gucht, J., Paluch, E., & Sykes, C. (2005). *Proc. Natl. Acad. Sci. USA*, *102*, 7847.
[9] Cook, P. R. (2001). *Principles of Nuclear Structure and Function*, Wiley: New York.
[10] Humphrey, D., Duggan, C., Saha, D., Smith, D., & Kas, J. (2002). *Nature*, *416*, 413.
[11] Nedelec, F., Surrey, T., & Karsenti, E. (2003). *Curr. Opin. Cell Biol.*, *15*, 118.
[12] Storm, C., Pastore, J. J., MacKintosh, F. C., Lubensky, T. C., & Janmey, P. A. (2005). *Nature*, *435*, 191.
[13] Marenduzzo, D., Orlandini, E., Cates, M. E., & Yeomans, J. M. (2008). *J. Non-Newt. Fluid Mech.*, *149*, 56; Marenduzzo, D., Orlandini, E., & Yeomans, J. M. (2007). *Phys. Rev. Lett.*, *98*, 118102.
[14] Beris, A. N. & Edwards, B. J. (1994). *Thermodynamics of Flowing Systems*, Oxford University Press: Oxford.
[15] Olmsted, P. D. & Goldbart, P. M. (1992). *Phys. Rev. A*, *46*, 4966.
[16] Olmsted, P. D. & David Lu, C.-Y. (1997). *Phys. Rev. E*, *56*, 55; (1999). *ibid*, *60*, 4397.
[17] de Gennes, P. G. & Prost, J. (1993). *The Physics of Liquid Crystals, 2nd ed.*, Clarendon Press: Oxford.
[18] Marenduzzo, D., Orlandini, E., Cates, M. E., & Yeomans, J. M. (2007). *Phys. Rev. E*, *76*, 031921.
[19] Thoumine, O. & Ott, A. (1997). *J. Cell. Sci.*, *110*, 2109.
[20] Uhde, J., Keller, M., Sackmann, E., Parmegiani, A. & Frey, E. (2004). *Phys. Rev. Lett.*, *93*, 268101.
[21] Succi, S. (2001). *The Lattice Boltzmann Equation*, Oxford University Press.
[22] Denniston, C., Marenduzzo, D., Orlandini, E., & Yeomans, J. M. (2004). *Phil. Trans. Roy. Soc. A*, *362*, 1745; Denniston, C., Orlandini, E., & Yeomans, Y. M. (2001). *Phys. Rev. E*, *63*, 056702; Marenduzzo, D., Orlandini, E., & Yeomans, J. M. (2004). *Phys. Rev. Lett.*, *92*, 188301; Care, C. M. & Cleaver, D. J. (2005). *Rep. Prog. Phys.*, *68*, 2665.
[23] Denniston, C., Orlandini, E., & Yeomans, J. M. (2001). *Phys. Rev. E*, *63*, 056702.
[24] Sulaiman, N., Marenduzzo, D., & Yeomans, J. M. (2006). *Phys. Rev. E*, *74*, 041708.